INDONESIAN JOURNAL ON GEOSCIENCE
Geological Agency
Ministry of Energy and Mineral Resources

Journal homepage: http://ijog.geologi.esdm.go.id
ISSN 2355-9314, e-ISSN 2355-9306

The Movement of Cimandiri Fault, Sukabumi, West Java: A Vertical Deformation Analysis Using DInSAR-True Vertical Displacement Method

Demi Stevany and Masita Dwi Mandini Manessa

Geography, Mathematics, and Natural Science Department, Universitas Indonesia

Corresponding author: demi.stevany21@ui.ac.id
Manuscript received: December, 9, 2022; revised: March, 23, 2023;
approved: January, 15, 2024; available online: February, 5, 2024

Abstract - If deformation is caused by earthquakes, it is necessary to map the area size and shape. Especially in Indonesia, which is situated within three main tectonic plates, the examination of risks and hazards is vital to establish the right measures for mitigating and minimizing the risk of earthquakes. Remote sensing is one of the best and most renewable methods for mapping deformation occurrences. DInSAR is a remote sensing technique that can be used to analyze deformation. This work employed the DInSAR technique to examine the Sentinel-1 A SLC-IW satellite and to investigate the deformation of the Cimandiri Fault in Palabuhanratu region, Sukabumi. Within one of these active faults, a magnitude of 4 Richter scale earthquake occurred on September 20th, 2022. Comparing satellite photos before and after the earthquake with the DInSAR yielded a large phase difference value centred on the Cimandiri Fault line with a phase range of -3,092 to 3,031. It indicates that the Cimandiri Fault is the earthquake epicentre on September 20th, 2022, in Palabuhanratu. The results of an investigation of the displacement value happening along the line of sight (LOS) fall between 0.105 and 0.672 m. Due to the incidence angle of the picture observation by satellite, the displacement must be adjusted since it is perpendicular to the ellipsoid referred to as the true vertical displacement. The fixed displacement finding of 0.126 to 0.806 m suggests that the region surrounding the Cimandiri Fault has risen. As GCP points, a number of GPS geodetic data points were incorporated from the field near the Bagbagan bridge, which was the site of the active fault. The outcomes demonstrated that the DInSAR true vertical displacement method can be used to determine the surface deformation.

Keywords: Cimandiri Fault, Sukabumi, DInSAR, Remote Sensing, Sentinel-1

© IJOG - 2024

How to cite this article:
Stevany, D. and Manessa, M.D.M., 2024. The Movement of Cimandiri Fault, Sukabumi, West Java: A Vertical Deformation Analysis Using DInSAR-True Vertical Displacement Method. *Indonesian Journal on Geoscience*, 11 (1), p.35-44. DOI: 10.17014/ijog.11.1.35-44

Introduction

Background

Indonesia will never be free from earthquakes, because geographically this region is located on part of Circum-Pacific Ring of Fire Belt, the most tectonic plate area in the world. This zone contributes to nearly 90% of earthquake occurrence on earth, and almost all of the are major earthquakes in the worl (Kramer, 1996). Several major earthquakes have occurred in the last ten years, and resulted in the loss of life and material that have affected the economic sector and development. The high seismic activity can also be seen from the records that in the period of 1900 - 2009 there were more than 8,000 main earthquake events with the magnitude of M > 5.0 (BNPB, 2019).

Earthquake processes involve physical activities of how energy interact during extreme conditions of breaking rocks or earth plates. So far, there is no theory that can be used to clearly describe the dynamics of rock rupture and the generation of earthquake energy. The precise location, time, and magnitude of an earthquake can not be predicted (Hidayat and Widi Santoso, 1997). Even in areas where a big earthquake is known to happen one day, the impact is still difficult to anticipate (BNPB, 2019). However, disaster risk reduction can be done by modeling disaster-prone areas and observing the movement of the earth plates with active satellite technology. Thus, appropriate policies and steps can be concluded to reduce the disaster risk (Teddy, 1995).

Recognizing the potential hazards is the first step in a disaster risk reduction, so this study describes an overview of the deformation hazard due to earthquakes in Palabuhanratu Bay area. Within the vision, principles, and commitments of a sustainable global development journey, the 2016 New Urban Agenda (NUA) explicitly mentions the disaster risk reduction (DRR) and resilience by promoting a proactive, risk-based approach to society. Global Assessment Report on Disaster Risk Reduction. Geneva, Switzerland, United Nations Office for Disaster Risk Reduction (UNDRR, 2019). Calls for sustainable natural resource management in cities are to promote DRR by developing DRR strategies and periodically assessing disaster risk. In addition, NUA expressed the commitment of member countries to increase the city resilience to disasters by adopting an approach that is in line with The Sendai Framework (UNDRR, 2019).

Learning from previous researches, this research will take several methods and analyses that are deemed necessary and effective for case studies of deformation due to future earthquakes. The method used and the analysis carried out is the DInSAR technique (Mabaquiao, 2021), looking at the displacement between the two SLC sentinel images (Muhammadi, A. *et al*., 2020), using the SRTM high verification technique for topographic phase removal (Tannu and Arvind, 2021). The initial results obtained from this processing are LOS (Line of Sight) displacements (Bayik, 2021) and are still not completely vertical. It is necessary to make displacements perpendicular to the earth surface completely without the influence of the incidence angle of observations from satellites, so that with geodetic mathematics the LOS displacement is converted into a true vertical deformation (Suhadha *et al*., 2021). The DInSAR method is suitable for nonlinear deformation monitoring, but it is not for a long-term deformation monitoring. To better explore the impact of errors other than spatiotemporal incoherence on the DInSAR results, two images with a time baseline of twelve days and a spatial baseline of 9 m were selected for DInSAR processing (Xu *et al*., 2022)

Cimandiri Fault

Sukabumi is an area in West Java Province that frequently experiences earthquakes. The earthquakes that occurred in Sukabumi were the result of a fault activity, namely the Cimandiri Fault and its segments. In the physiographic map, Sukabumi is included in the Bogor Zone which is an anticlinorium zone where the edges of the shelf with basins in turbidites accumulates, folds, and collides in the southern mountains of West Java (Bemmelen, 1949). Genetically, the Sukabumi area is divided into folded volcanic hills and mountains as well as the Sunda or Banda volcanic arc system with morphological appearance divided into morphological plains, wavy rather steep wavy, and steep hillsides. These two areas are separated by the existence of the Cimandiri Fault. This fault stretches from Palabuhanratu Bay continuously to the south of Sukabumi City and Cianjur Regency (Verstappen, 2000).

Cimandiri Fault is divided into five segments, those are Segments of Pelabuhan Ratu-Citarik, Citarik-Cadasmalang, Cicereum-Cirampo, Cirampo-Panglengseran, and Panglengseran-Gandasoli. The Cimandiri Fault is cut by several other faults such as the Citarik, Cicareuh, and Cicatih Faults (Gaffar, 2006). Based on the latest report from the Meteorology, Climatology, and Geophysics Agency (BMKG), an earthquake with a magnitude of 4.0 on the Richter Scale occurring on the 20^{th} September 2022 at 17:09:58 WIB was located at 7.05 South Latitude, 106.44 East Longitude, and a depth of 10 km. The epicentre was in the sea 14 km southwest of Sukabumi Regency. As can be seen in Figure 1, the red point is where the earthquake occurred.

Methods and Materials

DInSAR for Deformation Analysis

The modeling method for the deformation of the earth surface due to earthquakes used in this study is the Differential Interferometry Synthetic Aperture Radar (DInSAR) method (Cumming and Wong, 2005), which is a measurement of the phase difference between two SAR images on the same orbit (Ferreti *et al*., 2007). The two distances are compared to produce the phase difference between the two signals. The phase difference is represented by an interferogram which can be obtained by multiplying the phase by the complex conjugate.

The resulting interferogram consists of phase differences, so the results of the differences in the SAR pair are included in the deformation. It is important to note that the values in interferogram range from 0 to 2π or one wavelength cycle was used on a particular sensor from SAR imagery (Crosetto, 2002). The difference in the SAR phase between the master image on 12th September 2022 and the slave image on 24th September 2022 is one of the two main products in this study, which is then processed by adding and comparing with other variables and parameters in this study.

In this study, DInSAR processing was performed using the SNAP software, and the specific process is shown in Figure 2 assuming a set of Sentinel-1A SLC IW SAR images. This research uses product level 1 from Sentinel-1a SLC IW (Bourligot *et al*., 2016), because the product contains one image per subsweep, per channel, and polarization, making it easier for interpretation and lightening the workspace system workload. The polarization used is VV, which is vertical for transverse waves that are emitted and received by the satellite, because only vertical deformation was to be analyzed.

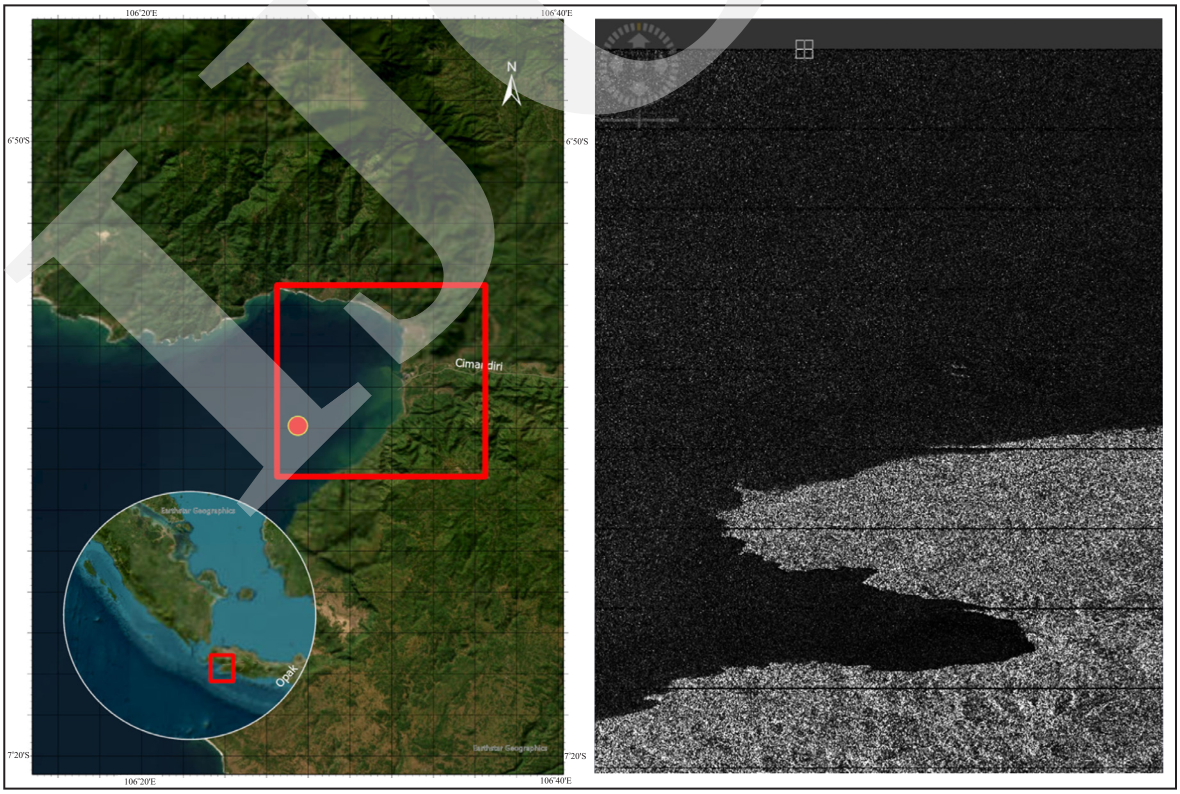

Figure 1. Researched area, Palabuhan Ratu, Sukabumi (right: Sentinel 1A SLC IW raw data, left: Esri Images).

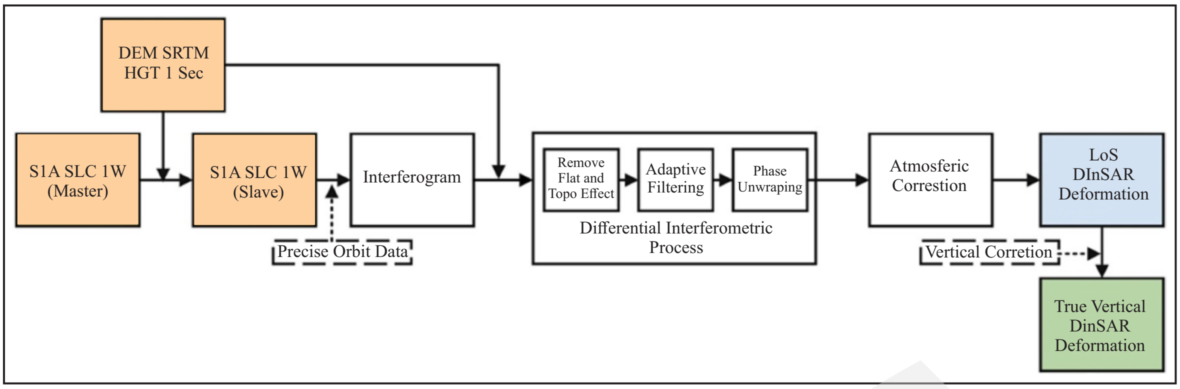

Figure 2. A flow chart of research method processes.

The Single Look Complex product has a spatial resolution that is dependent on the acquisition mode (ESA, 2022). In the table below (Table 1) for SM/IW/EW SLC products, the spatial resolution and pixel spacing are provided at the lowest and highest incidence angles. For WV SLC products, the spatial resolution and pixel spacing are provided for WV1 and WV2 images.

The SM and WV SLC products are sampled at natural pixel spacing, meaning that the pixel spacing is determined in azimuth by the pulse repetition frequency (PRF), and in range by the radar range sampling frequency. Thus, there will be slight variations around the orbit. Note that spatial resolution is a measure of a system ability to distinguish between adjacent targets, while pixel spacing is the distance between adjacent pixels in an image, measured in meter.

The data used shown in Table 2 as DInSAR input is Sentinel-1 Single Look Complex (SLC) Interferometric Wide (IW) mode, the image of which is associated with the same track and obtained with the same mode. Interferometric Wide (IW) is Sentinel-1 data acquisition mode which is suitable for interferometry applications (Sheng *et al*., 2009) due to its swath width and spatial resolution, especially for monitoring deformations. In addition, the availability of image data can be obtained free of charge (Sowter *et al*., 2016)

Sentinel-1A SLC IW SAR images acquired at the ordered time (before and after the earthquake) covering the studied area. The first step was to generate and coregistered SLC IW images with external DEM SRTM HGT 1 Sec data and pre-

Table 1. Acquisition Resolution Level-1 SLC

Mode	Resolution rg x az	Pixel spacing rg x az	Number of looks
SM	1.7x4.3 m to 3.6x4.9 m	1.5x3.6 m to 3.1x4.1 m	1x1
IW	2.7x22 m to 3.5x22 m	2.3x14.1 m	1x1
EW	7.9x43 m to 15x43 m	5.9x19.9 m	1x1
WV	2.0x4.8 m and 3.1x4.8 m	1.7x4.1 m and 2.7x4.1 m	1x1

Table 2. Data Used in Research

Data	Format	Source
Sentinel I A SLC IW	Raster	ESA
Data on the Epicenter of the Sukabumi Earthquake	Vektor	BMKG
Indonesian Fault Data	Vektor	BMKG
GPS Geodetic Data	Vektor	field observations

cision orbit data. Interferograms were achieved using the constraints on the perpendicular and temporal baselines, and the flattening and topographic effects were removed with the DEM. Then, adaptive filtering and phase unwrapping was used to obtain a series of unwrapped differential interferogram data. And then, a simple linear model was employed to remove the topography-dependent atmospheric phase. The value can be expressed as Formula 1 (Xu *et al.*, 2022):

$$\phi\text{diff} = \phi def + \phi\ topo_{res} + \phi atm\_res + \phi noise, \quad \text{......(1)}$$

where ϕdeff, ϕtopo-res, ϕatm-res, and ϕnoise represent the phase of land deformation, topographic errors, residual atmospheric artifacts, decorrelation, and thermal noise, respectively, along the radar of LOS (line of sight). The stages of elimination and reduction of the components of topographic errors, residual atmospheric artifacts, decor relations, and noise have been carried out as shown in Figure 2. The data processing was done using SNAP software by ESA (ESA, 2022). The step-by-step process that has been done is coregister the two products by using their orbits and a DEM by using the SRTM 1Sec HGT which has 30 m resolution instead of the default SRTM 3 sec which has 90 m resolution. Then, the Enhanced Spectral Diversity operator follows the Back-Geocoding operator. It first estimated a constant range offset for each burst using a small block of data in the centre of the burst, and then it estimated a constant azimuth offset. The estimates from all bursts were averaged to get the final constant range and azimuth offset for the whole image. Then, “Topographic Phase Removal” was to estimate and subtract the topographic phase from the deburst interferogram. After that, the “Multilooking” operator was used to reduce the inherent speckle noise that originally appeared to the SAR images, and square pixels and Goldstain Phase filtering would be obtained to reduce the phase noise. Then, Range Doppler Terrain Correction in the product containing the unwrapped interferogram and the one containing the displacement was carried out, to convert the RADAR coordinates into geographic. After removing and applying the components, the differentially exposed interferometric phase consists only of the deformation phase, and they can be converted into surface coatings, DInSAR results.

The SAR phase difference data, which is then called displacement data, will produce vertical LOS (line of sight) data that is still not perpendicular to the earth surface. Thus, it needs to be corrected to be true vertical, so that it is actual (Cuenca, 2013) with the Formula 2 below:

$$vertical\ displacemet = \frac{LoS}{cos\theta} \quad \text{....................(2)}$$

where the angle Θ is the incidence angle of the 1A SLC IW sentinel image. Due to the incidence angle of the picture observation by satellite, the displacement must be adjusted, so that it is perpendicular to the ellipsoid. This is referred to as true vertical displacement.

Result and Analysis

In this study, DInSAR processing was performed using the SNAP software. The specific process is shown in Figure 1 assuming a set of Sentinel-1A SAR images acquired at an ordered time, *i.e.* before and after the earthquake, that cover the studied area. The first result, which is the phase difference is shown in Figure 3. The red box shows the range of the highest phase difference during the earthquake in this study. Comparing satellite photos before and after the earthquake with the DInSAR yielded a large phase difference value centred on the Cimandiri Fault line with a phase range of -3.092 to 3.031. It indicates that the Cimandiri Fault was the earthquake epicentre on September 20th, 2022.

The red star (Figure 3) represents a place around the high phase difference located on the right side of the Cimandiri Fault line, which is the Bagbagan bridge (Figure 4a). The photo on the left shows the old yellow bridge that is no longer used, because it was damaged by the previous Cimandiri Fault earthquake, and was replaced by a new bridge on the right. The geodetic GPS data

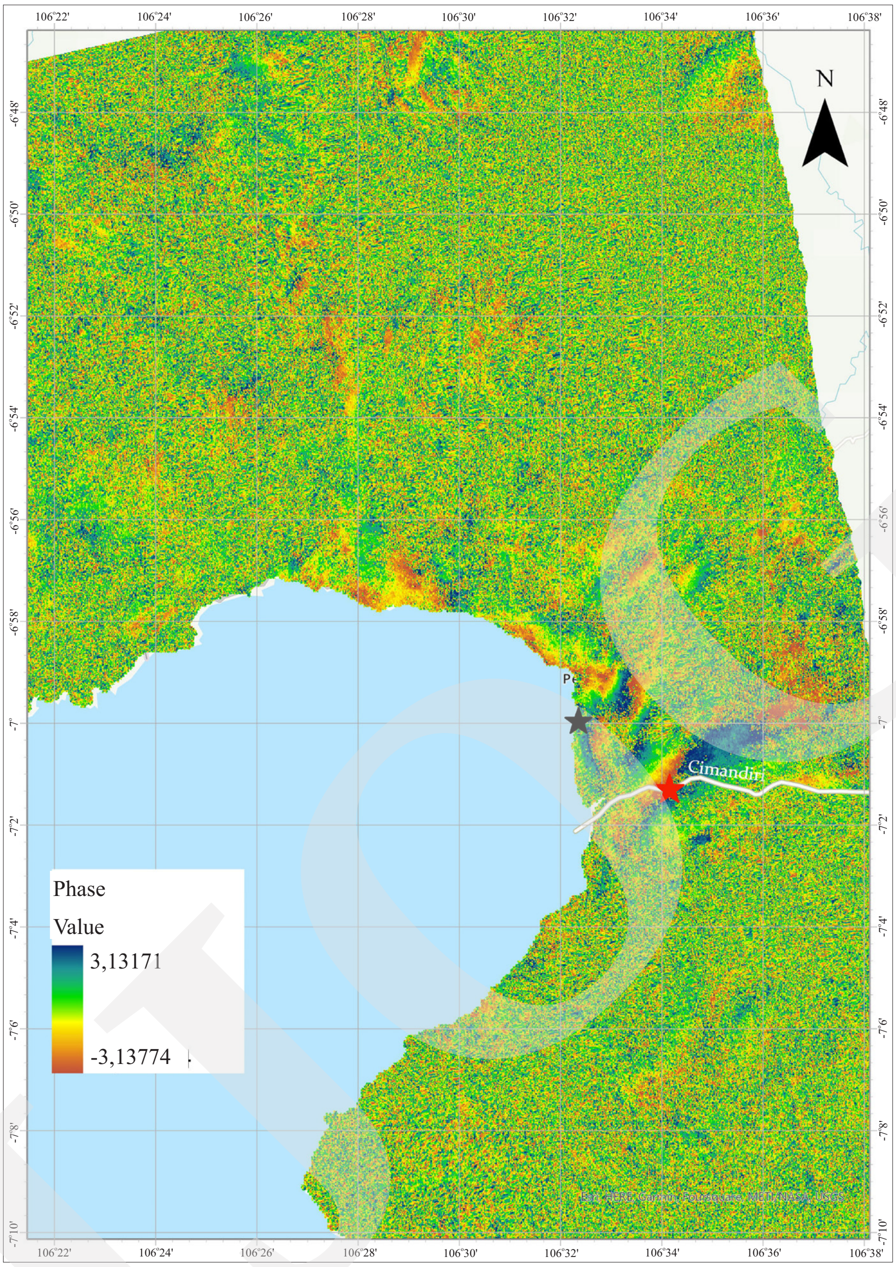

Figure 3. Phase difference.

Figure 4. Deformation occurred on huge phase range difference: a) Bagbagan bridge, b) Andira bridge.

was taken there as a ground control point (Ikbal *et al*., 2017). The black star (Figure 3) represents the Andira bridge (Figure 4b) which starts to show its deformation (Alatza *et al*., 2020), marked by the yellow rectangle.

The results of an investigation of the displacement value that happens along the line of sight (LOS) fall between 0.105 and 0.672 m (Fadhlurrohman, 2020). The fixed displacement is shown in Figure 5, a finding of 0.126 to 0.806 m suggesting the region surrounding the Cimandiri Fault has risen. There are two graphs in Figure 6. The upper one is before being corrected (in the form of a line of sight), then it is corrected so that it becomes the bottom graph, true vertical displacement. The graphs horizontally have the same value, but not vertically, as shown in the y value of both graphs. The true vertical is higher than LOS according to the Pythagorean triangle rule (Figure 7).

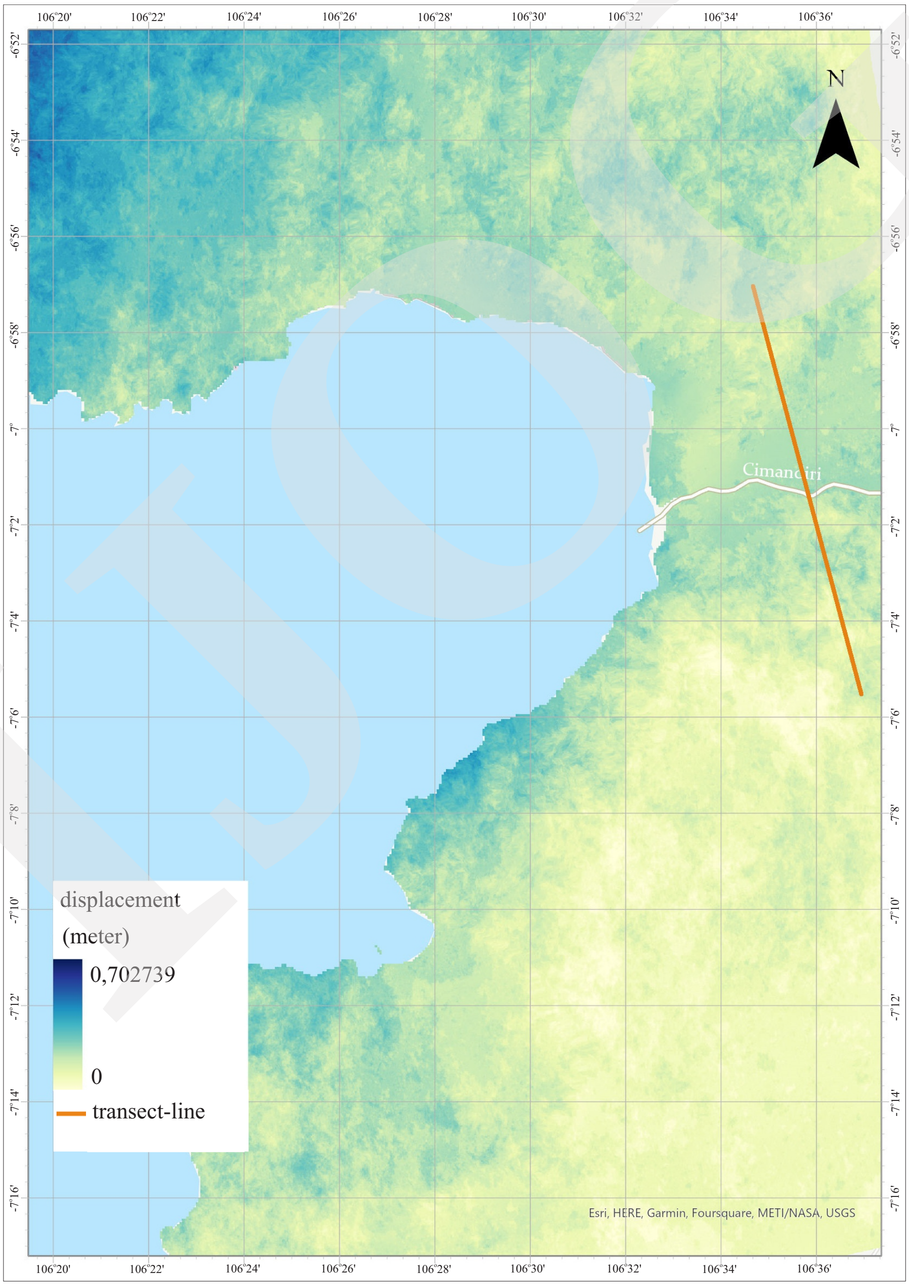

Figure 5. True vertical displacement on meter.

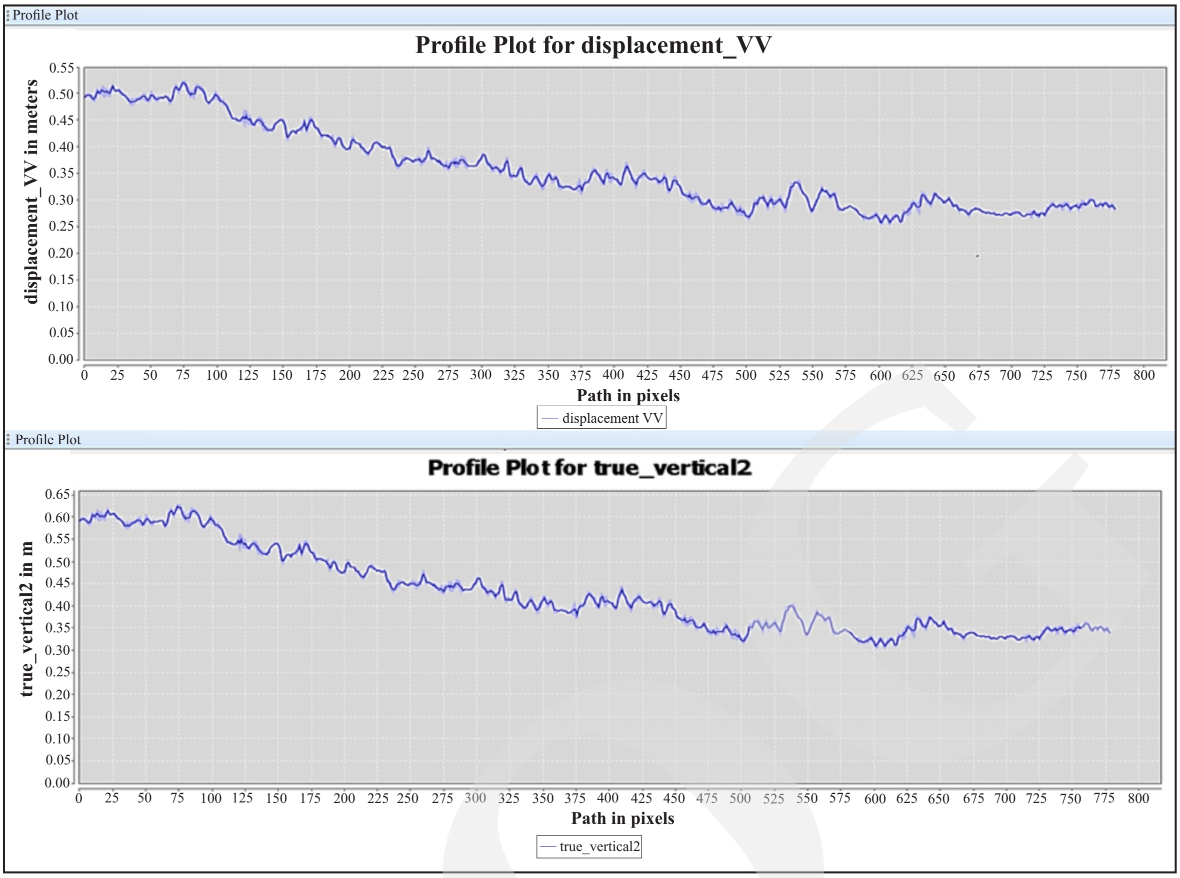

Figure 6. Profile plot (above: LOS, below: true vertical displacement) base on the transect line on Figure 5.

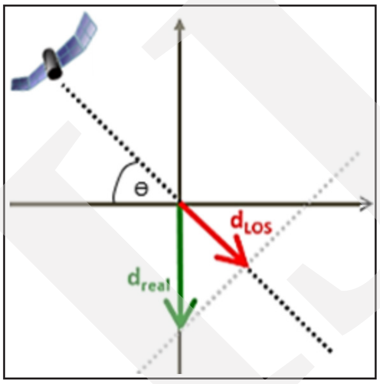

Figure 7. LOS and true vertical displacement on Pythagorean triangle rule.

Conclusions

In this research, DInSAR using SNAP software has been implemented to monitor the vertical deformation caused by the September 20th 2022 earthquake in Palabuhanratu, Sukabumi. The DInSAR result is in LOS displacement, which means converting to vertical displacement to get the actual displacement needed. A large phase difference value was centred on the Cimandiri Fault line with a phase range of -3.092 to 3.031. It indicates that the Cimandiri Fault is the earthquake epicentre on September 20th, 2022, in Palabuhanratu. Then, the fixed displacement finding of 0.126 to 0.806 m suggests that the region around the Cimandiri Fault has risen. The results demonstrated that the DInSAR true vertical displacement method can be used to determine surface deformation.

Acknowledgments

The authors would like to thank Geography, Mathematics, and Natural Science Department of Universitas Indonesia, ESA, NASA, and BMKG for providing the license of the SNAP Software, GPS Geodetic, workspace, supporting data, and implementation of this research. The street maps have been provided from Google.

References

Alatza, S., Papoutsis, I., Paradissis, D., Kontoes, C., and Papadopoulos, G.A., 2020. Multi-temporal InSAR Analysis for Monitoring Ground Deformation in Amorgos Island. *The 4th Joint International Symposium on Deformation Monitoring (JISDM 2019), Greece. Sensors,* 20, 338. DOI:10.3390/s20020338.

Badan Nasional Penanggulangan Bencana, 2019. *Risiko Bencana Indonesia*. https://bnpb.go.id/documents/irbi-15-1575660452.pdf.

Bayik, C., 2021. Deformation analysis of 2020 mw 5.7 Karlıova, Turkey, earthquake using DInSAR method with different incidence angle SAR data. *Arabian Journal of Geosciences,* 14, 273. DOI: 10.1007/s12517-021-06670-x.

Bemmelen, R.W. Van, 1949. *The Geology of Indonesia*. Martinus Nyhoff. Netherland: The Hague.

Crosetto, M., 2002. Calibration and validation of SAR interferometry for DEM generation. *Journal of Photogrammetric Remote Sensing*, 57, p.213-227.

Cuenca, M., 2013. *Improving radar interferometry for monitoring faultrelated surface deformation,* 81. Delft: NCG, Nederlandse Commissie voor Geodesie, Netherlands Geodetic Commission.

Cumming, I. and Wong, F., 2005. *Digital Processing of Synthetic Aperture Radar Data: Algorithms and Implementation*. Artech House.

European Space Agency (ESA), 2022. *Level-1 Single Look Complex*. User Guides, https://sentinel.esa.int/ [October 28th 2022].

Ferretti, A., Monti-Guarnieri, A., Prati, C., Rocca, F., and Massonnet, D., 2007. *InSAR Principles: Guidelines for SAR Interferometry Processing and Interpretation*. ESA Publication. The Netherlands.

Gaffar, E.Z., 2006. Deformasi Kerak Bumi Segmen-Segmen Sesar Cimandiri. *Prosiding Seminar Geoteknologi Peluang dan Peran Ilmu Kebumian Dalam Pembangunan Berkelanjutan*. Geotek LIPI.

Hidayat, N. and Widi Santoso, E., 1997. Gempa Bumi dan Mekanismenya. *Alami,* 2 (3), p.50-52.

Ikbal, M.C., Yuwono, B.D., and Amarrohman, F.J., 2017. *Analisis Strategi Pengolahan Baseline GPS Berdasarkan Jumlah Titik Ikat Dan Variasi Waktu Pengamatan*. *Tugas Akhir,* Teknik Geodesi Fakultas Teknik, Universitas Diponegoro, Semarang.

Kramer, S.L., 1996. *Geotechnical and Earthquake Engineering*. Prentice Hall, New Jersey, USA.

Lutgens, 1982. *Essentials of Geology*. A Bell & Howell Company, Colombus, Ohio 43216.

Mabaquiao, L.C., 2021. Insar-Based LOS Surface Deformation Comparison Of Metro Manila Before And After The January 2020 Taal Volcano Eruption. *Philippine Geomatics Symposium 2021*. https://doi.org/10.5194/isprs-archives-XLVI-4-W6-2021-201-2021.

Bourligot, M., Johnsen, H., and Piantanida, R., 2016. *Sentinel 1 Product definition, For Official Use*. ESA unclassified, MPC-S1.

Mohammadi A., Karimzadeh S., Kamran K.V., and Matsuoka, M., 2020. Extraction of Land Information, Future Landscape Changes and Seismic Hazard Assessment: A Case Study of Tabriz, Iran. MDPI. Switzerland. *Sensors,* 20, 7010; DOI:10.3390/s20247010.

Sheng, Y., Wang, Y., Ge, L., and Rizos, C., 2009. Differential Radar Interferometry and Its Application in Monitoring Underground Coal Mining-Induced Subsidence. *Gsem*, p.277-232.

Sowter, A., Amat, M.B.C., Cigna, F., Marsh, S., Athab, A., and Alshammari, L., 2016. Mexico City land subsidence in 2014-2015 with Sentinel-1 IW TOPS: Results using the Intermittent SBAS (ISBAS) technique, *International Journal of Applied Earth Observation and Geoinformation,* 52, p.230-242, ISSN 1569-8432.DOI: 10.1016/j.jag.2016.06.015.

Suhadha, A.G., Julzarika, A., Ardha M., Chusnayah, F., 2021. Monitoring Vertical Deformations of the Coastal City of Palu After Earthquake 2018 Using Parallel SBAS.

7th Asia-Pacific Conference on Synthetic Aperture Radar (APSAR), DOI: 10.1109/APSAR52370.2021.9688380.

Tannu and Arvind, 2021. Geoinformatics-based assessment of land deformation and damage zonation for Gorkha earthquake, 2015, using SAR interferometry and ANN approach. *SN Applied Sciences,* 3, 573. DOI: 10.1007/s42452-021-04574-9.

Teddy, B., 1995. Earthquake Phenomena. Two-day course on earthquake resistant design of building. Bangkok.

UNDRR, 2019. *Global Assessment Report on Disaster Risk Reduction*. Geneva, Switzerland, United Nations Office for Disaster Risk Reduction (UNDRR).

Verstappen, H., 2000. *Outline of The Geomorphology of Indonesia*. The Netherlands.

Xu, Y., Li, T., Tang, X., Zhang, X., Fan, H., and Wang, Y., 2022. Research on the Applicability of DInSAR, Stacking-InSAR and SBAS-InSAR for Mining Region Subsidence Detection in the Datong Coalfield. *Remote Sensing,* 14, 3314. DOI: 10.3390/rs14143314.